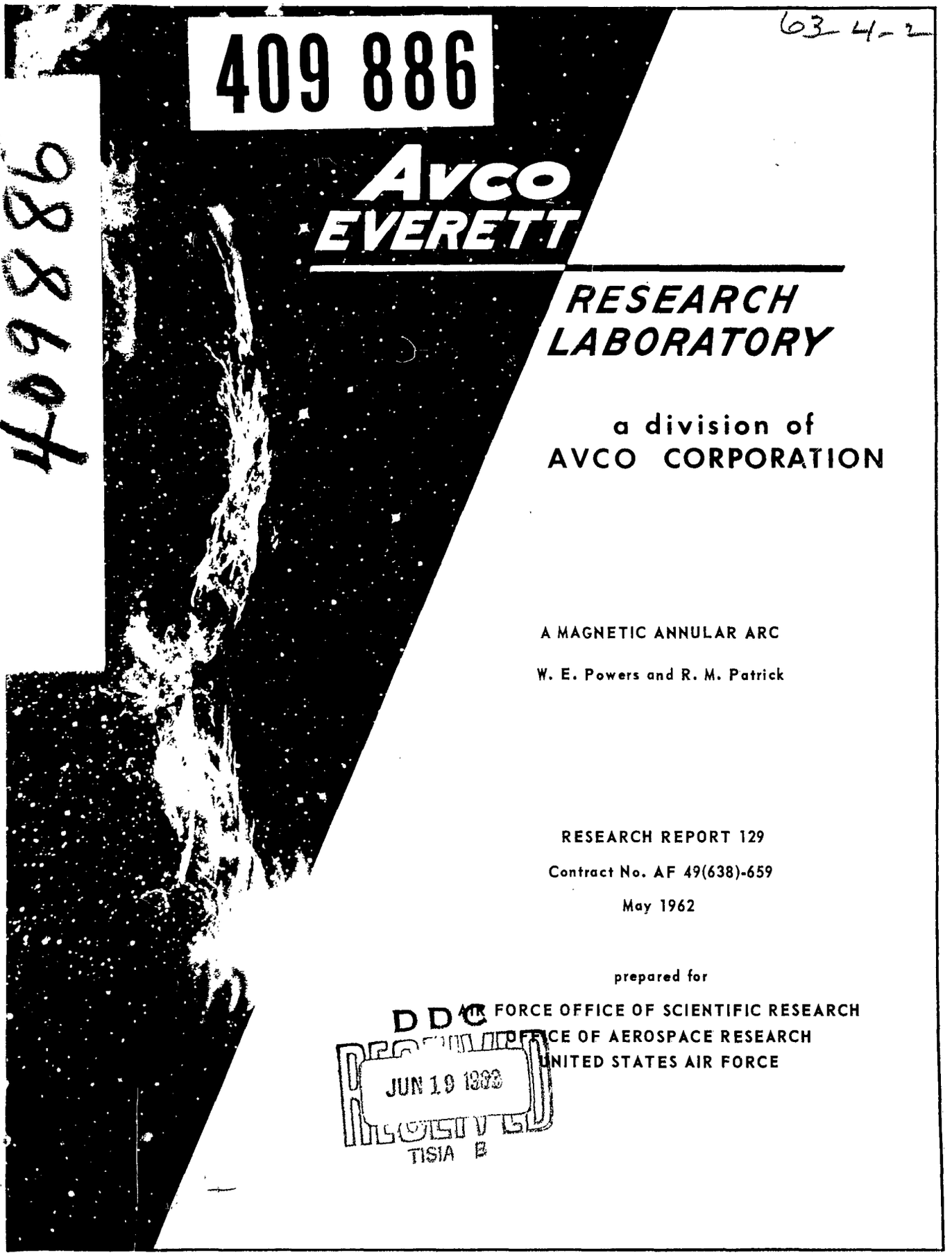

AVCO EVERETT RESEARCH LABORATORY

a division of
AVCO CORPORATION

A MAGNETIC ANNULAR ARC

W. E. Powers and R. M. Patrick

RESEARCH REPORT 129

Contract No. AF 49(638)-659

May 1962

prepared for

AIR FORCE OFFICE OF SCIENTIFIC RESEARCH
OFFICE OF AEROSPACE RESEARCH
UNITED STATES AIR FORCE

RESEARCH REPORT 129
(supersedes AMP 54)

A MAGNETIC ANNULAR ARC

by

W. E. Powers and R. M. Patrick

AVCO-EVERETT RESEARCH LABORATORY
a division of
AVCO CORPORATION
Everett, Massachusetts

Contract No. AF 49(638)-659

May 1962

prepared for

AIR FORCE OFFICE OF SCIENTIFIC RESEARCH
OFFICE OF AEROSPACE RESEARCH
UNITED STATES AIR FORCE
Washington, D.C.

Project: 9752
Task: 37521

406607

ABSTRACT

The performance characteristics of an annular arc configuration under the influence of a magnetic field have been experimentally analyzed, particularly with respect to the effects of tensor conductivity and jxB body forces. In this device the plasma conditions are such that the electrical conductivity is insufficient to prevent the diffusion of the plasma through the magnetic field, i.e., the magnetic Reynolds number was small. Experiments were conducted with this device using helium and argon at power levels up to 50 kw, magnetic field strengths to 10,000 gauss and particle densities of the order of $10^{16}/cm^3$ to $10^{17}/cm^3$. The electron gyro radius was smaller than the electron mean free path, i.e., $\omega_e \tau_e > 1$, where ω_e is the gyro frequency, and τ_e is the time between collisions for electrons. The impedance of the arc in helium was found to vary linearly with $\omega_e \tau_e$. The existence of a circulating azimuthal Hall current was also demonstrated. A yaw probe was employed to measure the angle of the flow due to the jxB Lorentz forces. A good agreement was found between the measured rotation in argon and the predicted value obtained from momentum considerations.

A. Introduction

The behavior of an annular D.C. arc formed by a radial current between two co-axial electrodes with a uniform axial magnetic field in the direction of the plasma flow (Fig. 1) is reported in this paper. In this device the plasma conditions are such that the electrical conductivity is insufficient to prevent the diffusion of the plasma through the magnetic field. The plasma need only be slightly ionized and the bulk of the energy invested in the plasma is obtained from the jxB Lorentz forces which act throughout the volume of the plasma.

Various studies[1,2] have shown the applicability of electro-thermal devices such as the arc for generating high-energy plasma streams that can be used as high velocity wind tunnels and as propulsion devices. These continuous duty direct current plasma accelerators are limited to operation below temperatures at which excessive thermal ionization is encountered. This is usually a condition corresponding to an ultimate plasma velocity of about 15,000 meters/second. Above this large unrecoverable energy investments in ionization and large losses to the walls due to conduction by hot mobile electrons occur. In addition, as the plasma temperature is increased, the electrical conductivity rapidly rises to the point where the electrode voltage drops are comparable to the resistive voltage drop across the main body of the plasma. To avoid these limitations, the use of crossed electric and magnetic fields to produce a relatively adiabatic acceleration cycle has been considered.[3] The magnetic annular arc offers the particular advantage of raising the directed energy level of the plasma at a rate which is independent of the axial flow velocity through the arc. This can result in the production of higher velocities in the nozzle exhaust with comparably low plasma temperatures. Hence, a reduction in the energy invested in ionization and dissociation, which cannot be recovered in an expansion nozzle, can be realized. The body force in the azimuthal direction imparts directed energy in rotation to the plasma.[4] This effect is small for low power levels where joule dissipation predominates and the device acts as a heater. As the conductivity increases at higher power levels, the body force work exceeds the dissipation and the plasma has more directed energy than internal energy. The energy in rotation may be subsequently converted to directed thrust in an expansion nozzle, yielding an increased plasma exit velocity which will exceed that attainable with an electrothermal device.

When $\omega_e \tau_e > 1$ (where ω_e = electron gyro frequency, and τ_e = time between collision), the transport properties of the plasma are no longer scalar quantities[5] and Hall currents exist in the $\vec{j}_r \times \vec{B}_x$ (azimuthal) direction.[6] This increases the magnetic annular arc impedance, helps to minimize the electrode losses, and also makes the attainment of very high plasma temperature possible without decreasing the plasma impedance. One further consequence is that electrons undergo complete gyro orbits around field lines, which are essentially parallel to the channel walls, between collisions.

Electron mobility perpendicular to the field is reduced, thereby reducing energy convection to the wall due to the electrons.

Experimental verification of the Hall current effect and the production of gas rotation for the magnetic annular arc is demonstrated in this report. The plasma conditions using helium and argon gas correspond to particle densities of the order of $10^{16}/cm^3$ to $10^{17}/cm^3$, power levels such that the average particle energy was 2 to 3 ev, and axial magnetic field strengths between 1,000 and 10,000 gauss. The field strength was sufficient to make $\omega_e\tau_e$ the product of the electron cyclotron frequency, ω_e, and the time between collisions for electrons, τ_e, greater than unity which caused large Hall currents.

In addition, azimuthal currents can produce directed energy in the expanding flow region. The magnetic field in the expansion nozzle can be parallel to the outside wall and have large radial components. The interaction between the azimuthal Hall currents and the radial field produces axial directed energy.

It is recognized that there are numerous aerodynamic and magnetic interaction problems associated with the design of the plasma exhaust nozzle. These deserve separate treatment and will be excluded from the present discussion.

B. The Magnetic Annular Arc Accelerator

1. Transport Properties

The transport properties of a highly-ionized plasma change when the electrons undergo one or more complete gyro orbits between collisons,[5] i.e., when $\omega_e\tau_e > 1$ (where ω_e is the gyro frequency for the electrons and τ_e is the mean time between collisions). When $\omega_e\tau_e >> 1$, the average distance the electrons diffuse across field lines per collision is equal to the gyro radius instead of the mean free path, as would be the case when $\omega_e\tau_e < 1$. Thus, for $\omega_e\tau_e > 1$, it is possible to reduce the electron mobility perpendicular to the magnetic field lines and reduce the heat conductivity and the electric conductivity by the factor $[1 + (\omega_e\tau_e)^2]^{-1}$. Equal ion and electron mobility is achieved when

$$\omega_e\tau_e \cong \left[\frac{m_I}{m_e}\right]^{1/4} \qquad (1)$$

where m_I and m_e represent the mass of the ions and electrons. For most gases this conditions is realized at $\omega_e\tau_e = 10$. This offers the possibility of controlling the electron heat transfer to the walls, which are aligned parallel to the magnetic field lines. The heat transfer due to electrons is important only for a plasma with a high degree of ionization.

In addition, when $\omega_e\tau_e > 1$ and an electric field is applied normal to the field lines, the electrical conductivity, σ, of the plasma is no longer a

scalar quantity. The electrical conductivity normal to the magnetic field lines[5] is proportional to $[1 + (\omega_e\tau_e)^2]^{-1}$ while the electrical conductivity along field lines remains unchanged. The electron drift in the direction perpendicular to both the magnetic and electric fields gives rise to Hall currents[6], and is proportional to $\omega_e\tau_e$.

2. Arc Impedance Characteristics

When an annular arc geometry is considered, such as shown in Fig. 1, the effects of the magnetic field discussed above are favorable for the arc operation. When $\omega_e\tau_e > 1$, closed Hall currents are generated in the $\vec{j}_r \times \vec{B}_x$ (azimuthal) direction. These currents are closed on themselves and no Hall potential exists.[4] One result of this is that the ratio of loop current, j_θ, to radial current flow across the electrodes, j_r, is equal to $\omega_e\tau_e$. Of particular importance is the fact that the impedance of the arc is affected by the magnetic field, since the radial conductivity is a function of $\omega_e\tau_e$. For the case when the plasma properties and current distribution is uniform across the channel, the radial conductivity of the plasma, σ_r, is as follows:

$$\frac{1}{\sigma_r} = \frac{1}{\sigma_o}\left(1 + \omega_e^2\tau_e^2\right) \qquad (2)$$

where σ_o is the plasma conductivity without B field. However, the current distribution in the magnetic annular arc is not uniform in the axial direction, because the length of the electrodes is small compared to the channel length (Fig. 2). The plasma conductivity in the axial direction is not changed by the magnetic field; therefore currents are free to flow downstream from the electrodes and these currents tend to short out the increased radial electric field caused by the decreased radial conductivity. An analysis of this problem for uniform plasma conductivity and finite electrodes was made and it was found that these axial currents extend further in the field direction by a factor $\omega_e\tau_e$ than when there is no axial field present. A brief description of this analysis is given in the Appendix. Hence there is a larger cross-section of plasma through which the current flows, and the arc impedance is reduced by a factor of $\omega_e\tau_e$. The results of the calculation for uniform $\omega_e\tau_e$ and conductivity showed that the arc impedance should be proportional to $[1 + (\omega_e\tau_e)^2]^{1/2}$ instead of $1 + (\omega_e\tau_e)^2$ which would be the case when no axial currents were allowed to flow. See Appendix.

The experimental case is such that the plasma is heated by the discharge and the plasma properties are not uniform throughout the channel. In particular, the incoming gas upstream of the discharge is at room temperature and will carry no current. The effect of increased axial currents should appear as an extension of the currents downstream from the electrodes (Fig. 2). Since there is a possibility of large axial currents along with large azimuthal currents, the arc impedance might show a dependence proportional to $\omega_e\tau_e$ instead of $\omega_e^2\tau_e^2$.

It is interesting to consider the effects on the thermal stability of the arc operation when $\omega_e\tau_e > 1$. For a slightly ionized gas, a higher

temperature corresponds to a higher degree of ionization and a lower value of $\omega_e \tau_e$ for constant magnetic field (see Figs. 3 and 4). Hence, if there is any concentration of current in the magnetic annular arc which produces a higher temperature and ionization, the value of $\omega_e \tau_e$ is decreased. This decreases the current density, which is proportional to $\omega_e \tau_e$, and thereby reduces the local dissipation. Therefore the Hall effects tend to stabilize the arc operation and produce a uniform energy and ionization level. This characteristic is not obtained in ordinary arcs, where an increased current corresponds to an increased temperature and conductivity, which in turn tends to increase the current further, resulting in thermal pinching and an unstable operation.

C. Experimental Techniques

The magnetic annular arc configuration, shown schematically in Fig. 1, consisted of a constant area annular geometry with a 3.2 cm diameter anode and a 1.6 cm diameter cathode. The L/D ratio was approximately 10. The anode was a water-cooled copper tube with a quartz insulating liner upstream of the arc plane. A thoriated tungsten electrode ring, 1-1/4 cm in length, was used on the cathode, which was water-cooled and insulated on each side of the electrode surface with quartz sleeves. On some of the later tests copper to copper electrodes were employed to circumvent the difficulty of maintaining intimate contact between the tungsten electrode rings and the water-cooled support tube due to thermal expansion effects. The performance characteristics of the arc were unaffected by this change. As shown in Fig. 1, the localized D.C. arc was used to heat cold gas which was subject to an essentially uniform axial magnetic field throughout the flow region. The arc dissipative power was supplied by a 50 kw D.C. variable supply. The D.C. current for the magnetic coils was supplied by a bank of batteries. The arc operation was continuous but dissipation in the coils restricted the duration of most runs to less than a minute.

The device has been operated with two magnetic field configurations. Initial studies of the arc impedance characteristics were made with a two coil configuration as shown in Fig. 1, each coil having 1240 turns. This arrangement provided an axial field distribution with a 5% decrease at the location of the arc. Without a local decrease in the magnetic field, the axial location of the arc was not stable. A second configuration of four coils, each with 310 turns, was used during investigations of the plasma conditions downstream of the arc (Fig. 10). This provided an essentially constant field for a length of 20 cm behind the arc.

The facility was instrumented to give arc voltage and current, coil current, gas mass flow, and calorimeter measurements of the heat transferred to the anode and cathode. Special probes were used to obtain the swirl angle, stagnation pressure and static pressure downstream of the arc, and flow Mach number. Other instruments used included: photomultiplier for observing the visible light intensity, high framing rate camera, search coils to examine the azimuthal Hall current intensity, and local calorimeter type heat transfer gauges.

D. Experimental Results

1. Arc Impedance Measurements

The visible radiation emitted by the arc-heated plasma was monitored with photomultipliers, a camera having a 2.5×10^{-5} second exposure time and a framing rate of 1000 per sec, and a camera with a 4×10^{-3} exposure time to give a still picture of the arc. The still picture is shown in Fig. 5 and was taken in argon. The radiation appeared to be asymmetric with no axial B field, indicating that the current distribution was not uniform around the annulus. However, with the axial B field used for the tests described here the radiation measured with the three techniques described above was uniform, indicating that the application of the axial field caused the plasma conditions to be uniform around the annulus.

A search coil diagnostic technique was employed to evaluate the existence of a circulating Hall current, j_θ. A 200 turn coil was placed outside the anode at the arc position as shown in Fig. 1. The oscillograph trace of the signal induced in this coil when the arc was turned off, with the B field left on, is shown in Fig. 6. The arc voltage and radial current decay are also shown. The coil signal provides a direct indication of the change in axial magnetic field due to the azimuthal j_θ current loops in the plasma. Integration of the signal showed that there was over 300 amps of circulating current in the vicinity of the pick-up coil. The value of $\omega_e \tau_e$ for this test was estimated to be approximately equal to 8. The ratio of the measured azimuthal current to radial current was equal to 3. We might expect the ratio of azimuthal to radial currents to be equal to $\omega_e \tau_e$ (Section B). However, the axial currents produce an extension of the arc downstream of the electrodes (Fig. 2). The search coil sensitivity is reduced as a result of this effect and a full measure of the perturbation of axial field due to the Hall current is not obtained. The signal level measured provides adequate assurance of the existence of the Hall effect.

The voltage and current of the magnetic annular arc have been measured for various power levels, mass flows, and magnetic field strengths. Typical results of these tests in argon are shown in Fig. 7. The impedance of the arc increased in this case by a factor of 15 when an axial magnetic field was applied.

The magnetic field geometry used for tests of the current voltage characteristics of the arc is shown in Fig. 1. This field was uniform in the vicinity of the electrodes to within 5 or 10%, depending on the coil spacing employed to produce a local dip for stabilizing the arc. The variation of the arc impedance for various input powers, mass flows, and magnetic field strengths was obtained. Some of these results are given in Fig. 7 for argon and Figs. 8 and 9 for helium. The mass flow for the data shown in Fig. 8 was held constant. The resistance with no magnetic field, R_o, was independent of the power input within the scatter of the data. This constant value of R_o indicates that additional power, exclusive of electrode losses, was invested in producing a higher degree of ionization in the helium plasma with

a small increase in temperature. The electrical conductivity, σ_o, is independent of the degree of ionization when the fraction of ionization is high enough so that the electron diffusion is governed by collisions with ions. This occurs at an ionization level above about 3×10^{-3} which is exceeded in the present tests. For a helium mass flow of 0.042 grams/sec, the power addition to the gas to raise the plasma temperature to 15,000°K with 1% ionization is 3.5 kw, with 0.25 kw for each additional percentage of ionization above this. Since the electron collision rate, τ_e, is governed by collisions with ions, τ_e is inversely proportional to the degree of ionization and thus to the power input. The results shown in Fig. 8 indicated that R/R_o was proportional to $\omega_e \tau_e$.

The influence of magnetic field strength on the operating characteristics of the magnetic annular arc at fixed power and mass flow are shown in Fig. 9. The experimental values of arc voltage, current, and resistance are presented for various magnetic field strengths. These data have been compared to the calculated behavior which predicts that the impedance ratio is proportional to $(1 + \omega_e^2 \tau_e^2)^{1/2}$. The enthalpy was obtained by measuring the power input and mass flow and subtracting the power loss at the electrodes due to electrode voltage drops. The electrode drop at the cathode was established by measuring both the heat loss to the water coolant at the cathode surface and the arc current. These measurements showed that the cathode voltage drop was about 6 to 8 volts. The anode drop in this device was more difficult to establish because of the integration of the anode losses in the cooling technique. The anode drop was assumed to be equal to the cathode drop and a total electrode drop of 14 volts was estimated.

Equilibrium was assumed and then plasma temperature was calculated which yields an electrical conductivity[5] σ_o, without the magnetic field. This value of σ_o at a power level of 20 kw and a current of 600 amperes in our geometry was used to calculate the arc impedance with no field. The no-field value was 0.45 ohms and since the impedance was predicted to be proportional to $(1 + \omega_e^2 \tau_e^2)^{1/2}$, the impedance as a function of applied field strength could be computed and the results of our calculation are given in Fig. 9. The $\omega_e \tau_e$ variation was obtained from Fig. 3 using the experimental pressure, magnetic field strength and plasma temperature.

The calculated values of the arc impedance with different B fields agree with the measured values shown in Fig. 9 within the scatter of the data.

2. Plasma Rotation

A second experiment was designed to show the separate effect of plasma thermal energy and directed energy. The directed energy in this experiment was due to the interaction of radial currents and the axial magnetic field which produced plasma rotation in the azimuthal direction.[4,7]

A new field coil geometry, employing four coils as shown in Fig. 10, was used for the investigation. This configuration avoided field gradients

downstream from the arc and provided an essentially constant B field for 20 cm of channel length beyond the arc.

The azimuthal velocity, v_θ, was detected by inserting a cylindrical yaw probe with appropriate seals through the water cooled anode wall. Low power tests yielding up to about 30° of swirl were made with a 3-1/2 mm diameter probe; for higher power levels a 6-1/2 mm diameter water cooled probe was necessary to handle the increased heat transfer. The point of insertion was between two coils 10 cm downstream of the arc. The probe was aligned normal to the plasma flow and spanned the annulus. It could be rotated so that two orifices at 90° included angle measured a differential pressure of sufficient sensitivity to establish the flow direction to within $\pm 1^\circ$. The probe was also used to determine the total pressure, when one of the orifices was aligned with the flow. Static pressure measurements were made on the inner and outer wall of the annulus, and these pressures were used to define the Mach number.

It can be shown from the momentum equation that the ratio of azimuthal velocity due to jxB body forces to axial velocity at any radius is

$$\frac{v_\theta}{u_x} = \tan\theta = \frac{(J_r x B_x)A}{2\pi r \dot{m} U \cos\theta} \tag{3}$$

where θ is the swirl flow angle relative to the axis, r the radius, J_r the radial current, B_x the magnetic field strength, A the cross-sectional area, $\dot{m}$ the mass flow and $U = (u_x^2 + v^2_\theta)^{1/2}$. All of these quantities are directly measurable, except U, which is obtained from the measured Mach number and plasma temperature.

Initial tests with helium showed no measurable level of swirl. However, calculations of the magnetic annular arc performance at low power levels (up to 20 kw total power) had predicted that this would be a small quantity. Since helium has a high ionization potential, (25 ev), a high energy per particle is required to produce a sufficiently high conductivity to make the rate of work done due to body forces comparable to the dissipation J^2/σ. The ionization potential for argon is 15 volts. To exploit this, a mixture of helium and argon, with 5% argon number density, was used. Measurable swirl angles were immediately obtained. Angles up to 33° were measured with the helium-argon mixture, implying a ratio of azimuthal to axial velocity $v_\theta/u_x = 0.65$.

Measurements were also made with pure argon gas; an example is shown in Fig. 11. Individual runs at each angle were necessary to establish the differential balance on the probe because of the low pressures involved. The correspondence obtained between hot and cold flow tests on the probe shows its suitability for measuring yaw angle.

The low density conditions (i. e., pressures of about 10^{-2} atmosphere) place the operation of the device in a low Reynolds number range. The Reynolds number based on pipe diameter was below 1000 for all tests. In addition. the device was made along for diagnostic reasons so appreciable viscous effects were expected. A total head survey in argon gave the result shown in Fig. 12. A parabolic profile fit to the data showed a fairly close correspondence, indicating a nearly developed Posieulle flow.

An estimate of the swirl angle decay in argon was made by calculating the viscous shear stress effect on the decay in angular momentum. This was done for the flow conditions in argon corresponding to a Reynolds number equal to 1000. The results of the calculation are given on Fig. 13, where both Eq. (3) (solid curve) and the estimate of swirl angle 10 cm downstream from the arc including viscous drag (dashed curve) are shown. The shear stress at the wall decreases the ratio between the angular and axial momentum because downstream from the arc there is no mechanism to maintain the angular momentum. It was necessary to eliminate the portion of the centerbody downstream of the arc to produce the highest swirl ratios shown. The swirl angles were measured at a position corresponding to 0. 7 of the anode radius at a point 10 cm downstream of the arc. The measured local impact pressure and the outside wall static pressure, p_{out} adjusted for centrifugal effects, were used to define the local Mach number at this station, from which the stream velocity was calculated. The centrifugal force resulting from the plasma rotation produces a radial pressure gradient which can be expressed by

$$p(r) = p_{in} + \int_{r_{in}}^{r} \frac{\rho(r)\, v_\theta^2(r)\, dr}{r} \tag{4}$$

where p_{in} is the innermost pressure free from centrifugal effect and ρ is the density. Because of difficulty in obtaining reliable static pressures on the inner body, the local static pressure was obtained by measuring the static pressure on the outside wall. Equation (4) can be written as

$$p(r) = p_{out} - \int_{r}^{r_{out}} \frac{\rho(r)\, v_\theta^2(r)\, dr}{r} \tag{5}$$

An estimate of both p(r) and ρ(r) was obtained by using Eq. (5) and assuming that the plasma temperature was constant throughout the channel, and that the azimuthal velocity was inversely proportional to r. The average plasma temperature was obtained from an energy balance, taking into account the power lost to the wall up to the measuring station, and subtracting this from the total input power to the plasma. The plasma enthalpy can be expressed

$$h_p(x) = \frac{P_{total}}{\dot{m}} - \frac{V_{electrode} I}{\dot{m}} - 2\pi r_o \int \dot{q}\, dx \tag{6}$$

where the integral extends from the electrodes to the measuring station, P_{total} is total power input, $V_{electrode}$ is the total electrode voltage drop, I is the arc current, $\dot{m}$ is the mass flow, r_o the channel radius, and $\dot{q}$ the measured heat loss to the walls. $\dot{q}$ was obtained by measuring the temperature rise of the water used to keep the walls cool, the heat loss as function of the distance from the electrodes was obtained from local heat transfer measurements. The local heat loss measurements were obtained with a water calorimeter gauge which is shown in Fig. 10. This plasma enthalpy, together with the measured static pressure, was used to calculate the average plasma temperature as a function of distance from the electrodes; this temperature was used to obtain the local sound speed. The azimuthal velocity distribution coincides with the distribution one obtains with radial current which is inversely proportional to r, a uniform magnetic field, and no momentum loss to the walls. First p(r) was computed using Eq. (5), using a mean value for the density, ρ. Then, $\rho(r)$ was computed using $\rho(r) = p(r)/RT$. This iteration process was carried out three times. The local Mach number was then calculated with this pressure and the measured impact pressure. The argon plasma densities for these tests were sufficiently low ($10^{16}/cm^3$) to prevent appreciable ion electron recombination between the electrodes and the measuring station during the time ($2 \cdot 10^{-5}$ seconds) required for the plasma to flow this distance. For this reason the value of $\gamma = 5/3$ corresponding to a monotomic gas was used. The temperature was used to estimate the axial velocity in Eq. (3).

The results of the experiments are plotted as solid circles in Fig. 13. For this plot the experimental measurements, θ, J_r, B_x, and $\dot{m}$, and the computed Mach number, speed of sound and axial velocity are presented in Table I. They show that the energy in rotation (directed energy) is comparable to the energy invested in plasma heating. The directed energy added to the plasma in this fashion, utilizing crossed electric and magnetic fields, provides a relatively adiabatic acceleration and avoids the large investure in dissociation or ionization energies which are characteristic of thermal arc heating.

Table I

θ Measured degrees	$\tan\theta$	$\frac{J_r B_x A}{2\pi r m U_x}$	J_r amps	B_x Weber/m^2	$\dot{m}$ kgs/sec	M	a m/sec	U_x m/sec
20.5	.374	.47	215	.70	2.4×10^{-3}	1.0	1350	1260
21	.384	.62	187	.575	1.0×10^{-3}	1.0	1750	1630
29	.554	.63	175	.67	1.29×10^{-3}	.98	1580	1360
44	.966	1.30	300	.955	1.5×10^{-3}	1.04	1880	1400
53	1.327	1.66	440	1.01	1.5×10^{-3}	1.46	1930	1710
57	1.54	1.82	435	1.03	1.5×10^{-3}	1.46	1940	1550

E. Conclusions

The experimental studies of the magnetic annular arc configuration presented in this paper permit the following conclusions:

1) The variation of the impedance of the annular arc in helium with power level, particle density, and magnetic field strength, has shown a close correspondence to a one-dimensional theory that predicts a linear variation of arc impedance with $\omega_e \tau_e$.

2) The discharge is stable when $\omega_e \tau_e > 1$ and the arc is uniform through the channel.

3) The possibility of imparting energy in rotation in the azimuthal direction has been determined to be in good agreement with the predicted action of jxB body forces.

Acknowledgement

The authors acknowledge the many helpful suggestions by various members of the Avco-Everett Research Laboratory during the course of the experiments, especially G.S. Janes, A.R. Kantrowitz, and H.E. Petschek. In particular, the authors are grateful for the analysis of the effect of tensor conductivity on the impedance of a plane electrode geometry which was written by F.J. Fishman and appears in the Appendix. They also wish to express thanks to A. LaPlante and M. Nastasia for their help in performing the experiment.

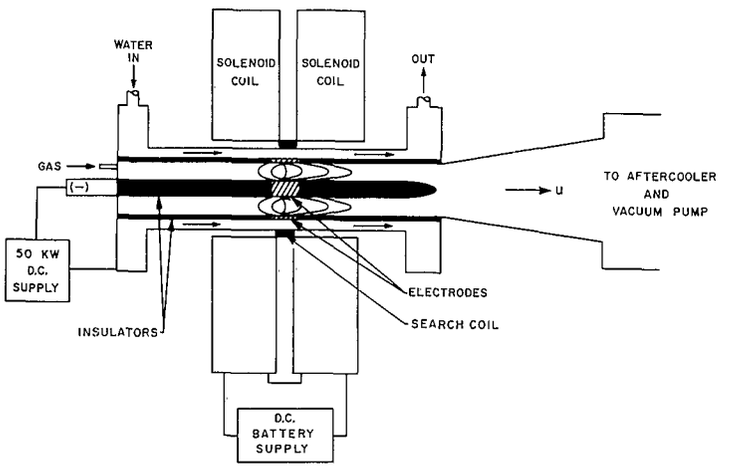

Fig. 1 Magnetic annular arc.

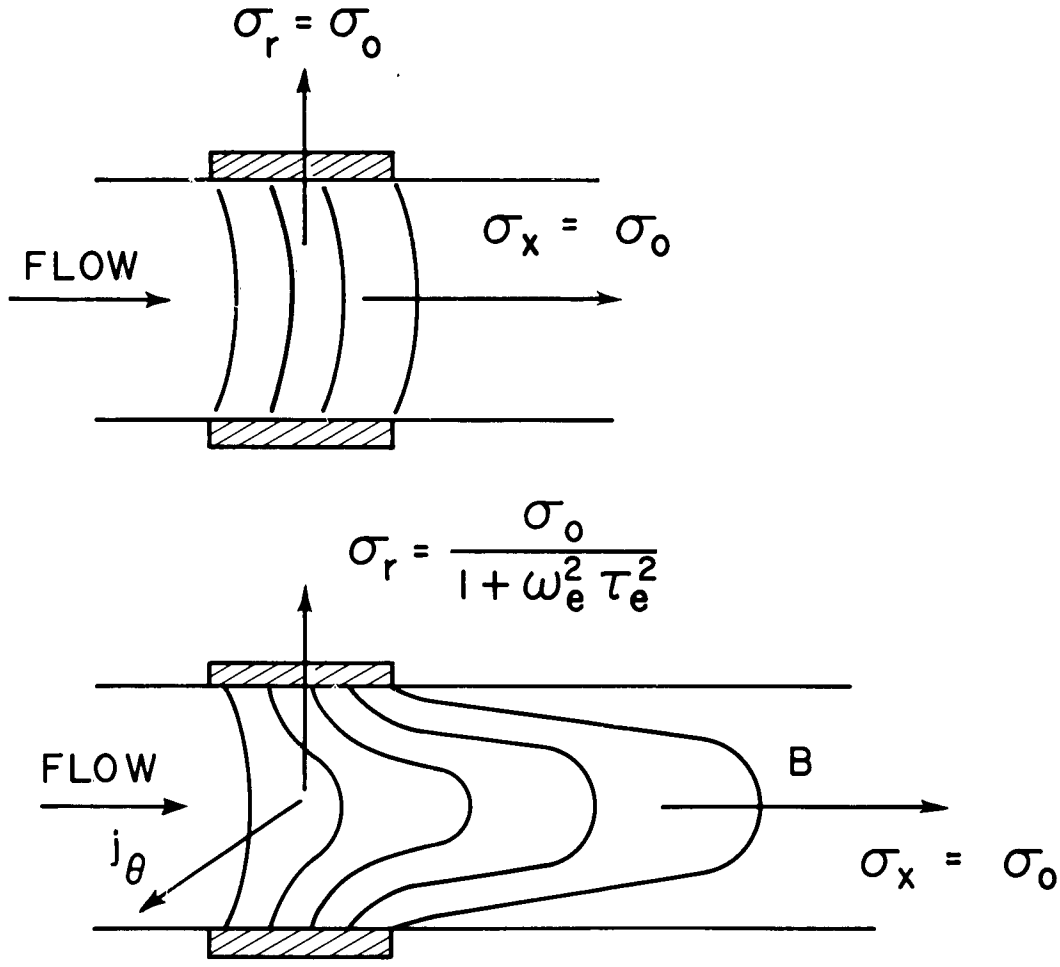

Fig. 2 Magnetic field effect on plasma conductivity and current flux pattern.

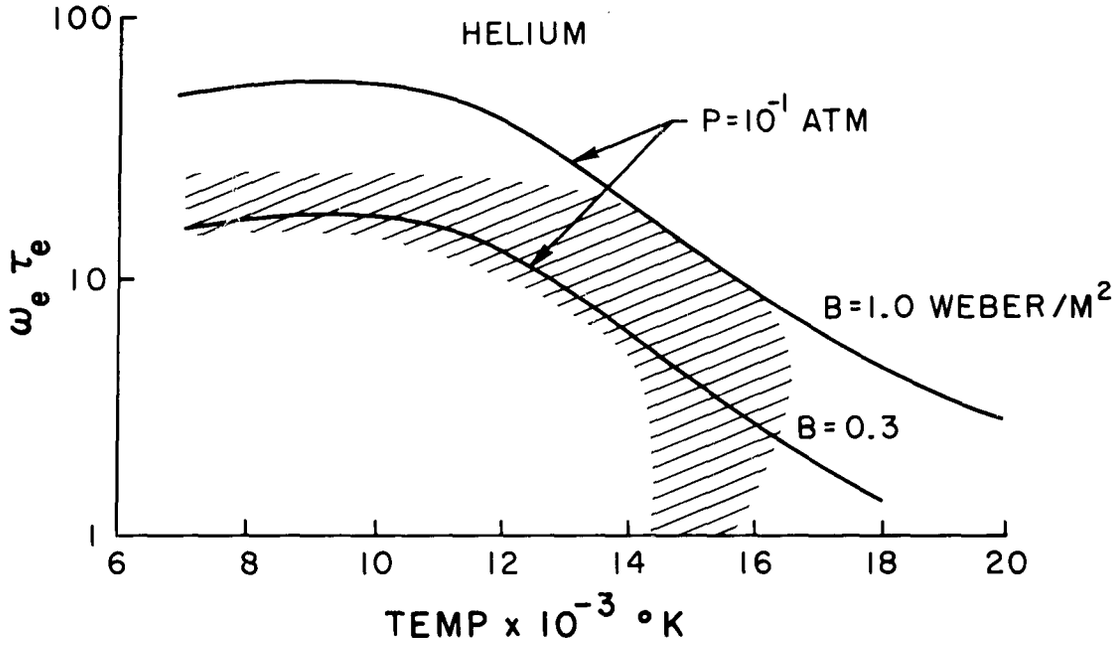

Fig. 3 Range in $\omega_e \tau_e$ with temperature in helium for the conditions of the experiments.

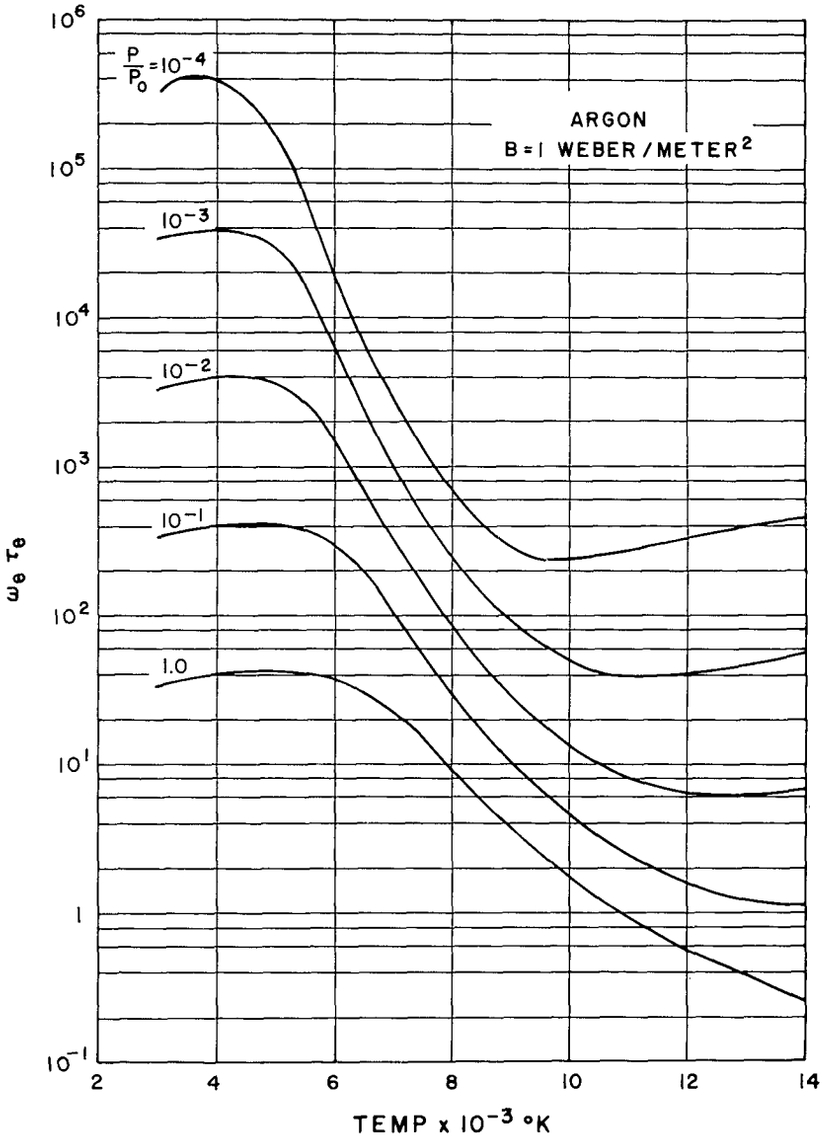

Fig. 4 Variation of $\omega_e \tau_e$ with temperature in argon for various pressures with applied magnetic field B = 1 Weber/meter^2.

B = 0

B = 10,000 GAUSS

Fig. 5 Photographs of the arc at 1/400 sec looking upstream with and without applied B field of 10,000 gauss.

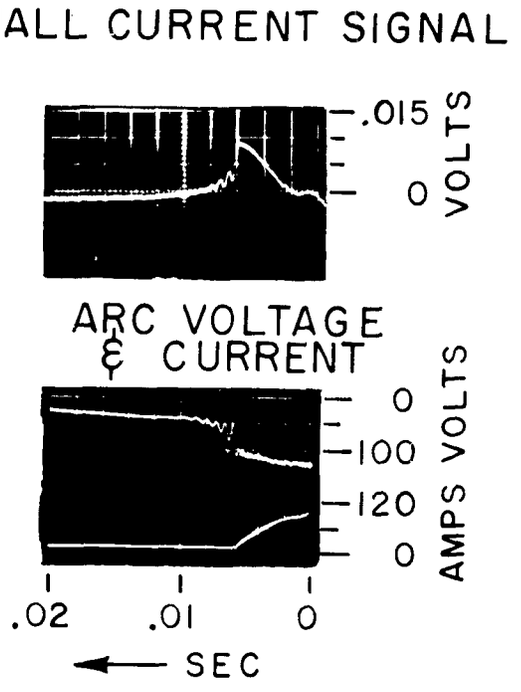

Fig. 6 Photograph of oscillograph signal trace obtained with a 200 turn search coil placed outside the anode at the arc position when the arc was turned off with the magnetic field left on. The arc voltage and current decay are shown in the lower oscillograph records. This measurement indicates the change in axial field, ΔB_x, due to j_θ current in the plasma.

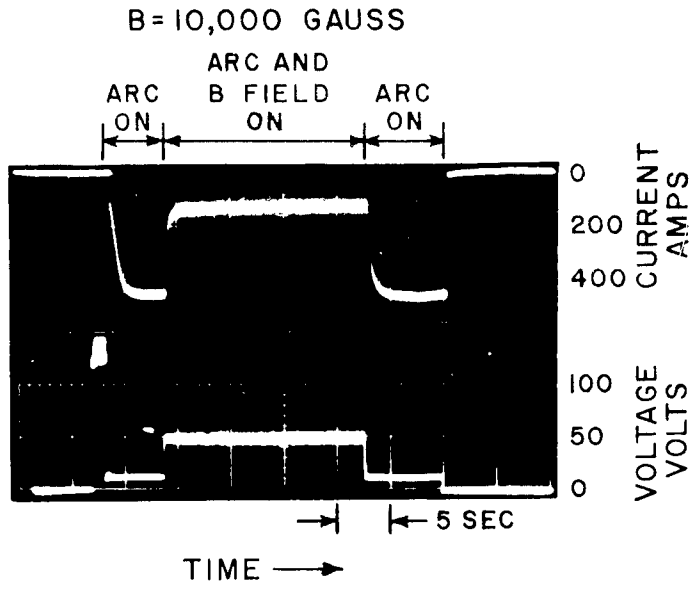

Fig. 7 Photograph of voltage and current oscilloscope traces for the magnetic annular arc showing the effects produced by turning the magnetic field on and off in argon gas.

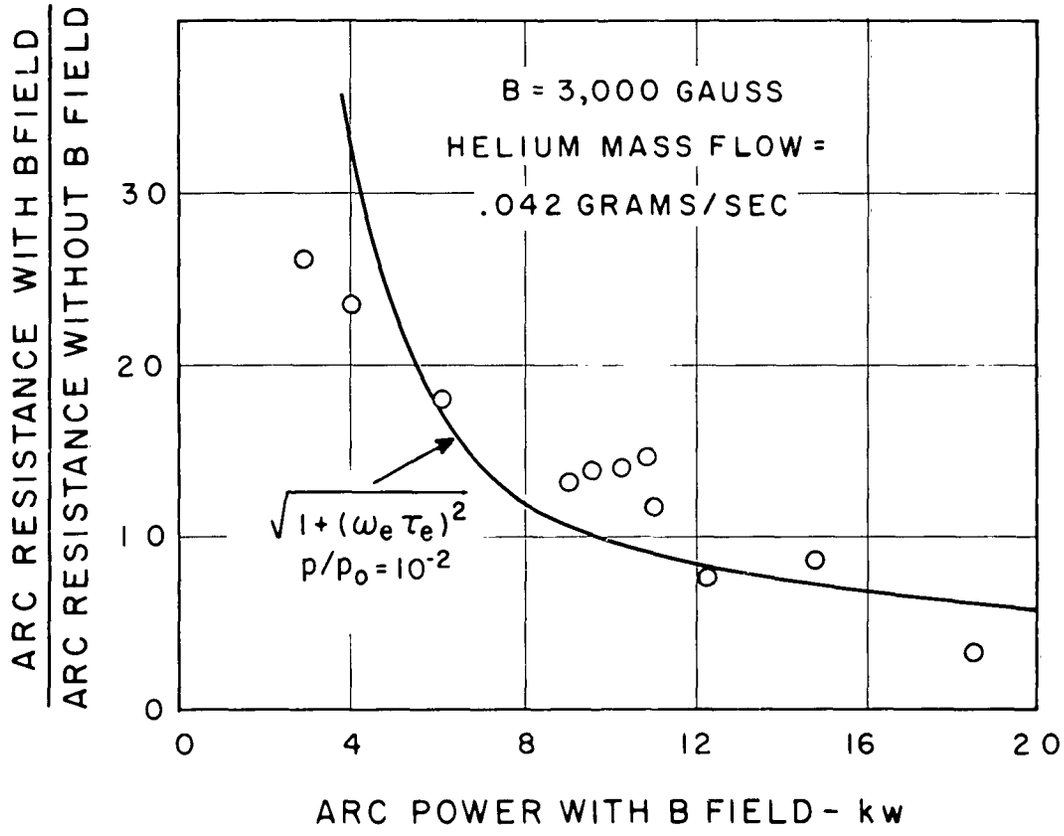

Fig. 8 Plot of the measured ratio of the resistance with and without magnetic field for the magnetic annular arc plotted against power input to the arc with B field applied. The arc resistance without B field was essentially constant.

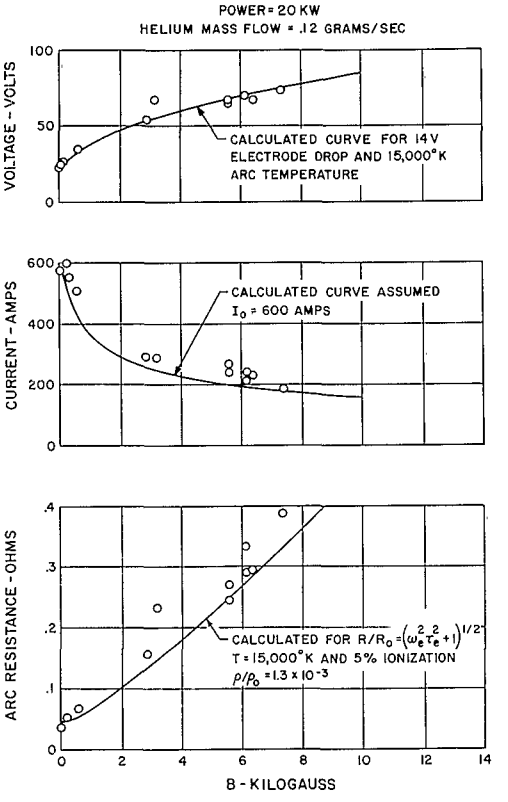

Fig. 9 Performance characteristics of the magnetic annular arc for fixed propellant flow and varying magnetic field.

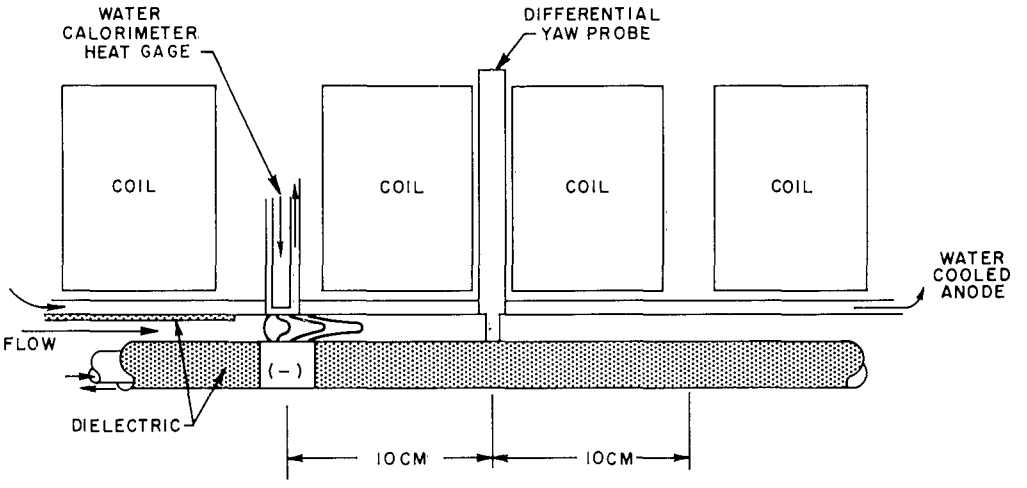

Fig. 10 Schematic of the four coil configuration used to provide an essentially uniform axial magnetic field for a distance of 20 cm downstream of the arc. The location of the arc and differential yaw probe employed for swirl angle measurements is shown.

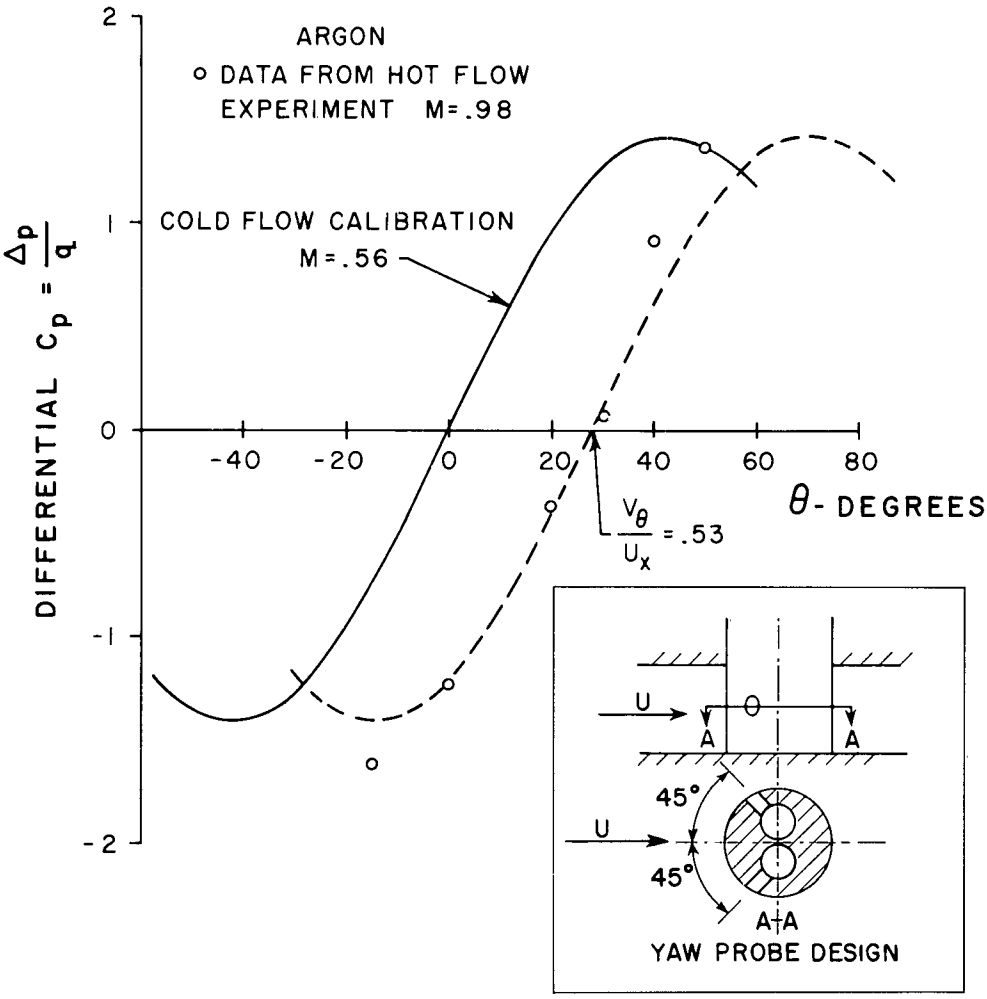

Fig. 11 Cylindrical yaw probe differential pressure coefficient versus angle relative to axis of the magnetic annular arc. The cold flow calibration curve has been displaced from zero and represented by a dashed curve to show the correspondence of the data to the anticipated probe response. The probe pressure difference has been non-dimensionalized to the dynamic pressure $q = 1/2\rho U^2$.

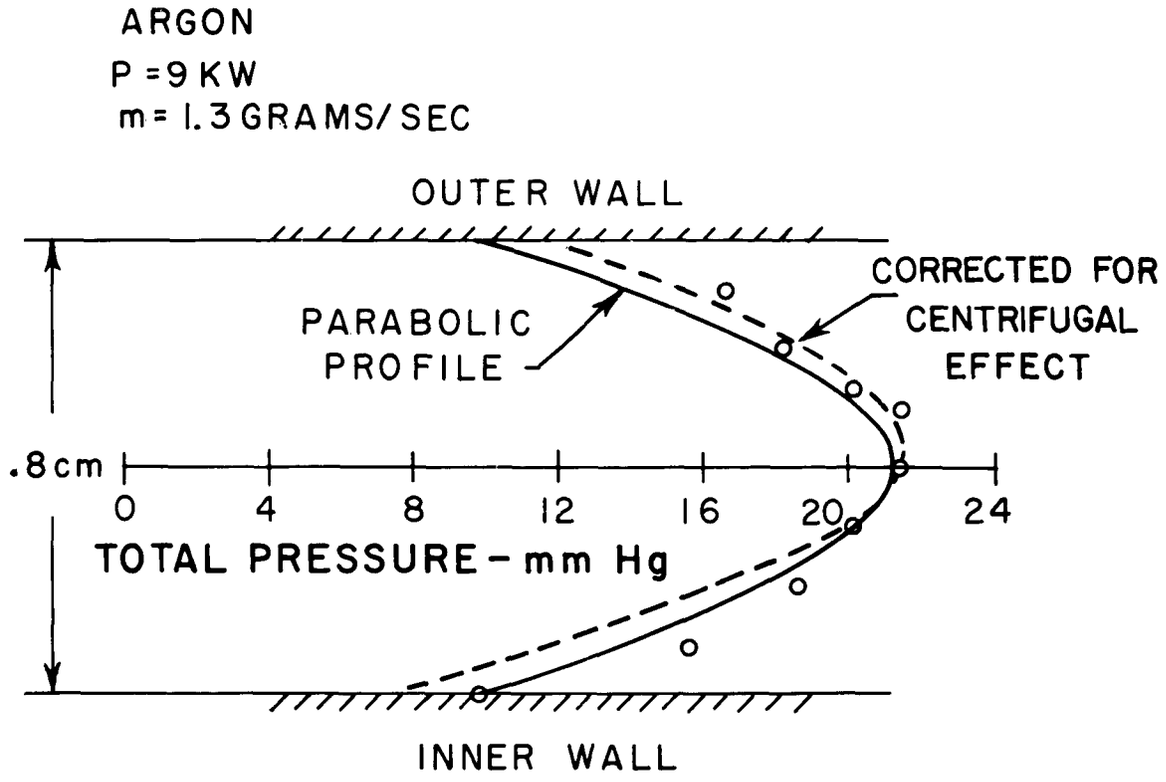

Fig. 12 Total pressure survey across the annulus with argon at a point 10 cm downstream of the arc showing a parabolic profile match to the data which would represent fully developed Poisieulle type flow and the modified profile corrected for centrifugal effect.

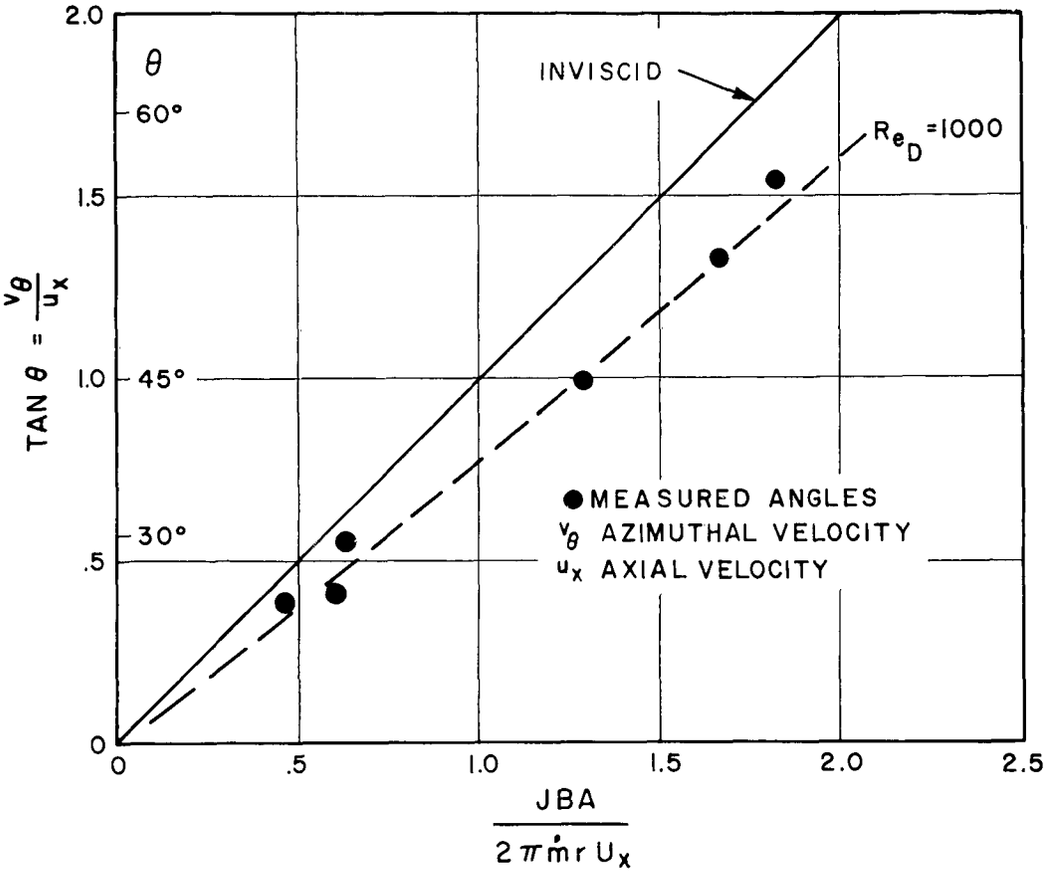

Fig. 13 Plot of the tangent of the flow angle 10 cm downstream from the electrodes. The measurements are plotted and shown as solid circles; the calculated inviscid curve was obtained by using a momentum balance between the flow and measured J x B forces. The dashed curve shows the angular momentum loss due to viscous drag at the experimental conditions. The abscissa of this plot is total angular momentum due to measured J x B forces normalized with respect to the axial flow momentum. J is the total measured current; B is the axial field; A is the channel area, u_x the axial velocity, $v\theta$ the azimuthal velocity, and r the radius where the measurements were taken.

APPENDIX

Useful insight into the effect of the magnetic field on the magnetic annular arc impedance can be obtained from consideration of the following idealized problem. A plasma is confined in the two-dimensional channel formed by the planes $y = 0$ and $y = h$. (Fig. A-1). These channel walls are insulators except for an electrode strip in the region $0 < X < \Delta$ on each wall; a potential difference V is maintained between these electrodes. A uniform magnetic field B, with only a component in the X direction, fills the channel. The plasma is taken to be uniform and at rest (or to have an arbitrary motion in the X direction; such motion along the magnetic field is not coupled to the other aspects of the problem). The currents produced in the plasma because of the potential applied across the electrodes are assumed to be small so that they do not modify the magnetic field or the plasma state. Because of the magnetic field the plasma currents are not parallel to the electric field and a generalized Ohm's law must be used to describe conduction phenomena; since there is no flow across the magnetic field, this Ohm's law may be assumed to have the form:

$$\vec{j} = \sigma_0 \left(1 + \omega_e^2 \tau_e^2\right)^{-1} \left[\vec{E} - \omega_e \tau_e \, \vec{E} \times \hat{X} + (\omega_e \tau_e)^2 (E \cdot \hat{X}) \, \hat{X} \right] \qquad (A\text{-}1)$$

where $\hat{X}$ is a unit vector in the magnetic field direction. The flow is assumed steady, so that $\nabla \times \vec{E} = 0$ and a potential ϕ may be defined such that $\vec{E} = -\nabla \phi$. Charge conservation requires $\nabla \cdot \vec{j} = 0$; this condition applied to Eq. (A-1) yields

$$\left(1 + \omega_e^2 \tau_e^2\right) \frac{\partial^2 \phi}{\partial X^2} + \frac{\partial^2 \phi}{\partial Y^2} = 0 \qquad (A\text{-}2)$$

where we have further assumed that there is no component of the electric field in the Z direction.

Introducing the transformation

$$X' = X \left(1 + \omega_e^2 \tau_e^2\right)^{-1/2} \qquad (A\text{-}3)$$

reduces Eq. (A-2) to Laplace's equation

$$\frac{\partial^2 \phi}{\partial X'^2} + \frac{\partial^2 \phi}{\partial Y^2} = 0 \, .$$

This transformation also modifies the geometry of the experiment in that the electrodes are reduced in width by the factor $(1 + \omega_e^2 \tau_e^2)^{-1/2}$, as indicated in Fig. A-2. On the electrode surfaces there can be no tangential electric field so that $\partial \phi / \partial X = 0 = \partial \phi / \partial X'$ for $y = 0, h$; $0 < X' < \Delta (1 + \omega_e^2 \tau_e^2)^{-1/2}$. The condition that there be no current into the insulating walls can be written with the aid of Eq. (A-1) as $\partial \phi / \partial Y = 0$ for $y = 0, h$; $X' < 0$, $X' > \Delta (1 + \omega_e^2 \tau_e^2)^{-1/2}$. This two-dimensional potential problem is conveniently solved by a complex variable mapping technique. The potential distribution is determined by the mapping from the plane $Z = X' + iY$ to the plane $\zeta = \phi + i \psi$, where ζ is defined as that analytic function whose real part is ϕ. The geometry in the ζ plane is evident from the boundary conditions; the electrodes map to lines of constant ϕ while the insulating walls are surfaces of constant ψ (since $\partial \phi / \partial Y = - \partial \psi / \partial X'$): the resulting rectangular configuration is indicated in Fig. A-3.

The mapping is conveniently done as two mappings of the Schwartz-Christolffel form, the first of which maps the channel from the Z plane to the upper half t plane, and the second which maps this half plane into the rectangle in the ζ plane; the t plane is indicated in Fig. (A-4). The first transformation has the form

$$\frac{dZ}{dt} = \frac{C_1}{t} \qquad t = e^{-\pi Z h^{-1}} \tag{A-4}$$

where the constants have been chosen to map the left edges of the electrodes to the points $t = \pm 1$. The right edges go to the points $t = \pm a = \pm \exp \left\{ - \pi \Delta h^{-1} (1 + \omega_e^2 \tau_e^2)^{-1/2} \right\}$. Mapping the interior of the rectangle in the ζ plane onto the upper half t plane is accomplished by the transformation

$$\frac{d\zeta}{dt} = C_2 (t^2 - 1)^{-1/2} (t^2 - a^2)^{-1/2}. \tag{A-5}$$

Performing the indicated integration is not necessary to obtain the relative electric field or current distribution, since

$$\frac{d\zeta}{dZ} = \frac{\partial \phi}{\partial X'} - i \frac{\partial \phi}{\partial Y} = - (1 + \omega_e^2 \tau_e^2)^{1/2} E_X + i E_Y \tag{A-6}$$

and $d\zeta/dz$ may be evaluated directly from (A-4) and (A-5). However, the constant C_2, which describes the magnitude of the fields has yet to be determined (from the symmetries of the problem, it can be seen to be real).

C_2 may be related to the applied potential across the electrodes, V by forming the integral $\int \vec{E} \cdot d\vec{l}$ from any point on one electrode to any point on the other. A convenient choice of path is from the right edge of the lower electrode along the lower wall to $X' = \infty$ (where E vanishes); the path back along the upper wall to the electrode provides an equal contribution. In the t plane this is the integral along the real axis from - a to 0;

$$V = 2\int_{\Delta(1+\omega_e^2\tau_e^2)^{-1/2}}^{\infty} E_X dX = 2\int_{-a}^{0} C_2\left[(1-t^2)(a^2-t^2)\right]^{-1/2} dt = 2\,C_2\,K(a) \qquad (A\text{-}7)$$

where K (a) is the complete elliptic integral of the first kind. Similarly, the total current between the electrodes is the integral of the normal current density across any surface completely separating them. A convenient choice is the plane Y = h/2, which transforms to the imaginary axis in the t plane. Using Eqs. (A-1), (A-4), (A-5) and (A-6) yields

$$J = \frac{\sigma_0}{1+\omega_e^2\tau_e^2}\int_{-\infty}^{\infty} E_Y(Y = h/2)\,dX = \frac{\sigma_0 C_2}{(1+\omega_e^2\tau_e^2)^{1/2}}\int_{i)}^{\infty} \frac{dt}{\left[-(1-t^2)(a^2-t^2)\right]^{1/2}}$$

$$= \frac{\sigma_0 C_2 K\left(\sqrt{1-a^2}\right)}{(1+\omega_e^2\tau_e^2)^{1/2}} \qquad (A\text{-}8)$$

Thus the electrical resistance seen at the electrodes is

$$R = V\,J = \frac{2\,(1+\omega_e^2\tau_e^2)^{1/2}\,K\left\{\exp(-\pi\delta)\right\}}{\sigma_0\,K\left\{\left[1-\exp(-2\pi\delta i\right]^{1/2}\right\}} \qquad (A\text{-}9)$$

where

$$\delta = \Delta\, h^{-1}\,(1+\omega_e^2\tau_e^2)^{-1/2}$$

The limiting values of the impedance for both large and small values of δ are easily obtained from Eq. (A-9) and their interpretation yields physical insight into magnetic effects on impedance. These limits are:

$$\delta \to \infty \qquad R \to \frac{(1+\omega_e^2\tau_e^2)\,h}{\sigma_0\left[\Delta + 2\,(\ln 2)\,\pi^{-1}\,(1+\omega_e^2\tau_e^2)^{1/2}h\right]} \qquad (A\text{-}10)$$

$$\delta \to 0 \qquad R \to 2\,(1 + \omega_e^{\,2}\tau_e^{\,2})^{\,1/2}\,(\pi\sigma_0)^{-1}\,\ln\,(8\pi^{-1}\,\delta^{-1}). \qquad \text{(A-11)}$$

When δ is large, the current can be considered to flow uniformly in a region the width of the electrode plus two end fringes of width $(\ln 2)\pi^{-1}$ $(1 + \omega_e^{\,2}\tau_e^{\,2})^{1/2}h$. When the end correction may be neglected, then the resistance depends on the magnetic field only through lowered conductivity across the field, and hence is proportional to $1 + \omega_e^{\,2}\tau_e^{\,2}$. However, the fringing current may be described as a parallel admittance that decreases more slowly with magnetic field; since the region over which the currents fringe increases as $(1 + \omega_e^{\,2}\tau_e^{\,2})^{1/2}$, the admittance contributed by them decreases only as $(1 + \omega_e^{\,2}\tau_e^{\,2})^{-1/2}$.[8] Further, since the expression for R of Eq. (A-10) is a good approximation to (A-9) even for values for $\delta \sim 0.1$, a range of conditions exist under which the overall resistance varies as $(1 + \omega_e^{\,2}\tau_e^{\,2})^{1/2}$. For still small values of δ the effective current fringing width becomes less than $(\ln 2)\pi^{-1}\,(1 + \omega_e^{\,2}\tau_e^{\,2})^{1/2}h$ because of the increased current densities at the electrodes. Expression (A-11) can be understood in terms of currents fringing from a fine source in the X' - Y plane, yielding the characteristic logarithmic potential variation; the combination of the decreased conductivity in the Y direction with the increased fringing introduces the factor $(1 + \omega_e^{\,2}\tau_e^{\,2})^{1/2}$ into (A-11).

These considerations are borne out by the results of the exact expression (A-9) which are plotted in Fig. A-5. The ratio of the resistance in the presence of a magnetic field to the resistance of the same geometrical configuration but with $\omega_e\tau_e = 0$ is plotted against $\omega_e\tau_e$ for two values of Δ/h. For comparison purposes the curves $(1 + \omega_e^{\,2}\tau_e^{\,2})^{1/2}$ and $1 + \omega_e^{\,2}\tau_e^{\,2}$ are also plotted.

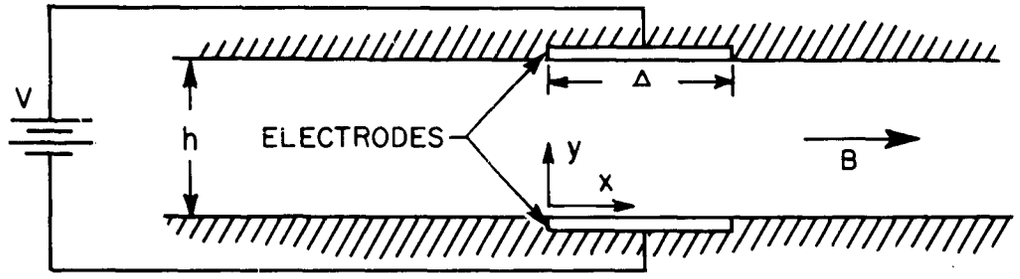

Fig. A-1 Geometry of idealized problem for investigating effect of magnetic field on arc impedance.

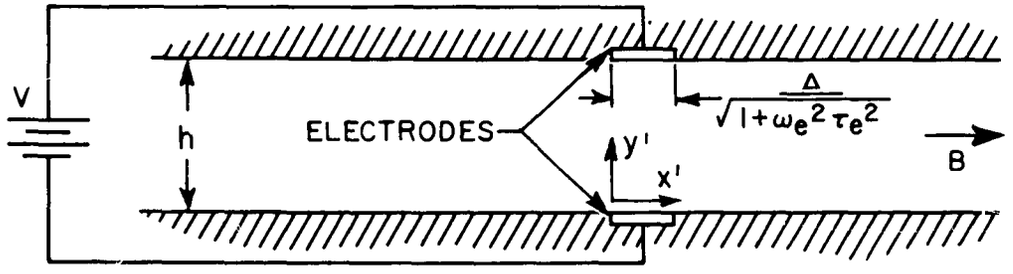

Fig. A-2 Channel geometry in transformed plane in which electric potential satisfies Laplace's equation.

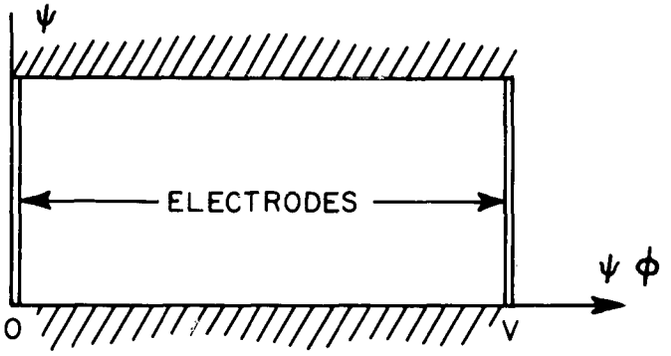

Fig. A-3 Channel region mapped onto complex potential plane.

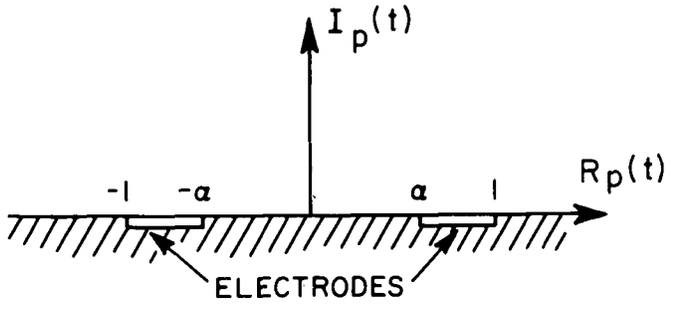

Fig. A-4 Intermediate t plane. The electrodes are the surfaces of the real axis such that $\alpha < |t| < 1$ where $\alpha = \exp\left\{-\pi \Delta h^{-1}(1+\omega_e{}^2 \tau_e{}^2)^{-1/2}\right\}$.

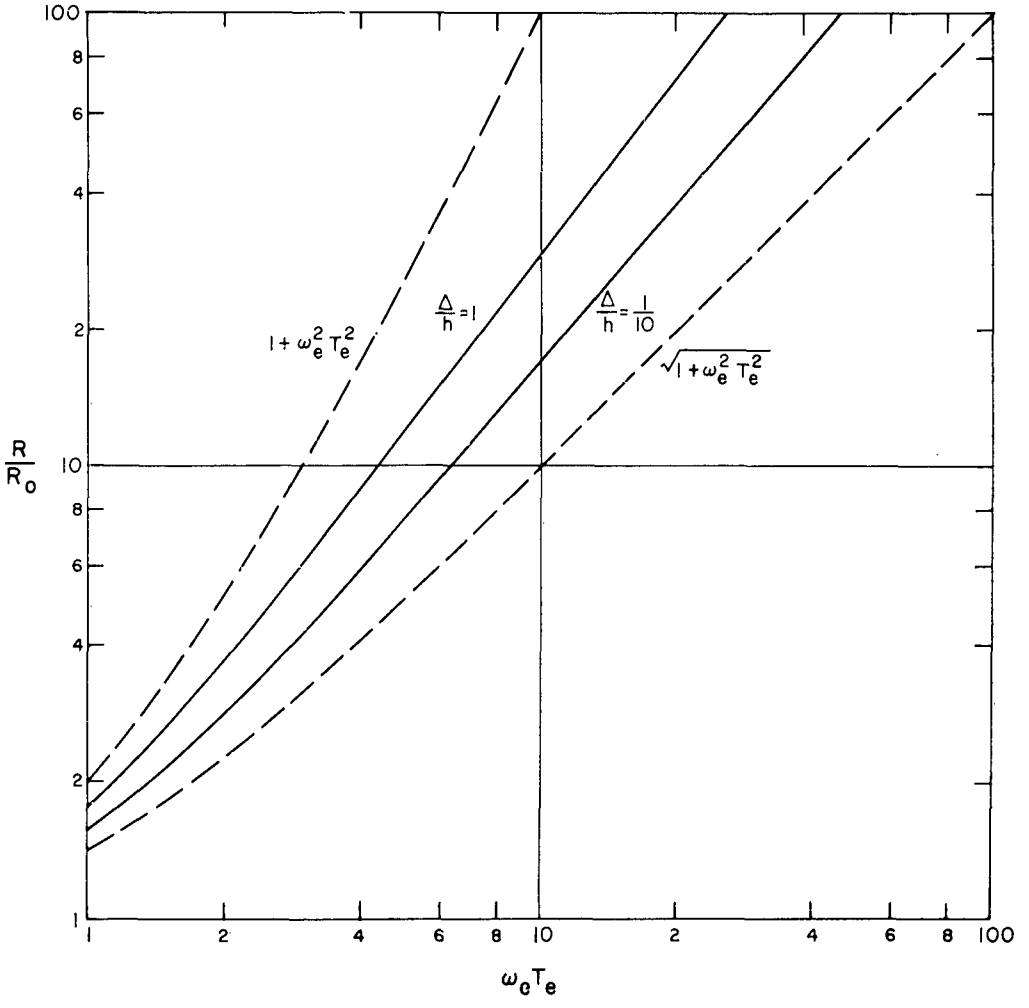

Fig. A-5 Ratio of resistance between electrodes with and without magnetic field.

REFERENCES

1. Brogan, T. R., "The Electric Arc Wind Tunnel - A Tool for Atmospheric Re-entry Research," ARS Journal, Vol. 29:648, September, 1959.

2. Giannini, G. M., "The Arc Jet." Presented at the Second Symposium on Advanced Propulsion Concepts, Boston, Mass., October, 1959.

3. Janes, G. S., "Magnetohydrodynamic Propulsion," Avco-Everett Research Laboratory, Research Report 90, August, 1960.

4. Powers, W. E. and Patrick, R. M., "A Magnetic Annular Arc." Paper presented at the Second Symposium on the Engineering Aspects of Magnetohydrodynamics, University of Pennsylvania, Philadelphia, Pa., March 9 and 10, 1961.

5. Spitzer, L., The Physics of Fully Ionized Gases, Interscience, 1956.

6. Patrick, R. M. and Brogan, T. R., "One-Dimensional Flow of an Ionized Gas Through a Magnetic Field," J. Fluid Mech., 5:289, February, 1959.

7. Hess, R. B., "Experiments and Theory for Continuous Steady Acceleration of Low Density Plasma," Proceedings XIth International Astronautical Congress, Stockholm, 1960, Springer-Verlag, 1960.

8. This effect and the transformation Eq. (A-3) which implies it were first pointed out by M. Litvak (private communication).

Avco-Everett Research Laboratory, Everett, Massachusetts
A MAGNETIC ANNULAR ARC, by W. E. Powers and R. M. Patrick. May 1962. 33 p. incl. illus. (Project 9752; Task; 37521) (Avco-Everett Research Report 129)
(Contract AF 49(638)-659)

Unclassified report

The performance characteristics of an annular arc configuration under the influence of a magnetic field have been experimentally analyzed, particularly with respect to the effects of tensor conductivity and jxB body forces. In this device the plasma conditions are such that the electrical conductivity is insufficient to prevent the diffusion of the plasma through the magnetic field, i. e., the magnetic Reynolds number was small. Experiments were conducted with this device using helium and argon at power levels up to 50 kw, magnetic field strengths to 10,000 gauss and particle densities of the order of $10^{16}/cm^3$ to $10^{17}/cm^3$. The electron gyro radius was

(over)

UNCLASSIFIED

1. Arcs, magnetic annular.
2. Plasma physics.
3. Accelerators.
I. Title.
II. Powers, W. E.
III. Patrick, R. M.
IV. Avco-Everett Research Report 129.
V. Contract AF 49(638)-659.

UNCLASSIFIED

Avco-Everett Research Laboratory, Everett, Massachusetts
A MAGNETIC ANNULAR ARC, by W. E. Powers and R. M. Patrick. May 1962. 33 p. incl. illus. (Project 9752; Task; 37521) (Avco-Everett Research Report 129)
(Contract AF 49(638)-659)

Unclassified report

The performance characteristics of an annular arc configuration under the influence of a magnetic field have been experimentally analyzed, particularly with respect to the effects of tensor conductivity and jxB body forces. In this device the plasma conditions are such that the electrical conductivity is insufficient to prevent the diffusion of the plasma through the magnetic field, i. e., the magnetic Reynolds number was small. Experiments were conducted with this device using helium and argon at power levels up to 50 kw, magnetic field strengths to 10,000 gauss and particle densities of the order of $10^{16}/cm^3$ to $10^{17}/cm^3$. The electron gyro radius was

(over)

UNCLASSIFIED

1. Arcs, magnetic annular.
2. Plasma physics.
3. Accelerators.
I. Title.
II. Powers, W. E.
III. Patrick, R. M.
IV. Avco-Everett Research Report 129.
V. Contract AF 49(638)-659.

UNCLASSIFIED

smaller than the electron mean free path, i. e., $\omega_e r_e > 1$, where ω_e is the gyro frequency, and r_e is the time between collisions for electrons. The impedance of the arc in helium was found to vary linearly with $\omega_e r_e$. The existence of a circulating azimuthal Hall current was also demonstrated. A yaw probe was employed to measure the angle of the flow due to the jxB Lorentz forces. A good agreement was found between the measured rotation in argon and the predicted value obtained from momentum considerations.

UNCLASSIFIED

UNCLASSIFIED

smaller than the electron mean free path, i. e., $\omega_e r_e > 1$, where ω_e is the gyro frequency, and r_e is the time between collisions for electrons. The impedance of the arc in helium was found to vary linearly with $\omega_e r_e$. The existence of a circulating azimuthal Hall current was also demonstrated. A yaw probe was employed to measure the angle of the flow due to the jxB Lorentz forces. A good agreement was found between the measured rotation in argon and the predicted value obtained from momentum considerations.

UNCLASSIFIED